*Electronic Supplementary Information for*

# Enabling photocatalytic activity of [Ru(2,2′:6′,2″-terpyridine)₂]²⁺ integrated into a metal-organic framework

Dong Luo,[a,†] Tao Zuo,[a,†] Ji Zheng,[a] Zi-Hao Long,[a] Xue-Zhi Wang,[a] Yong-Liang Huang,[b] Xiao-Ping Zhou,[a,*] Dan Li[a,*]

[a] College of Chemistry and Materials Science, Guangdong Provincial Key Laboratory of Functional Supramolecular Coordination Materials and Applications, Jinan University, Guangzhou, Guangdong 510632, P. R. China

[b] Department of Chemistry, Shantou University Medical College, Shantou, Guangdong 515041, P. R. China

[†] These authors contributed equally to this work.

E-mail: zhouxp@jnu.edu.cn, danli@jnu.edu.cn

## Syntheses of the complexes

### General procedure

Starting materials, reagents, and solvents were purchased from commercial sources (Alfa Aesar, J&K, and TCI) and used without further purification. Fourier transform infrared (FT-IR) spectra were measured using a Nicolet Avatar 360 FT-IR spectrophotometer (vs = very strong, s = strong, m = middle, w = weak). Thermogravimetric analysis (TGA) was carried out in a nitrogen stream using Thermogravimetric analyses (TGA) were performed using a Thermo Scientific TGA 2 thermal analysis equipment under nitrogen current (20 mL min$^{-1}$) at a heating rate of 10 °C min$^{-1}$. Powder X-ray diffraction (PXRD) experiments were performed using a Rigaku Ultima IV X-ray diffractometer (Cu K$\alpha$, $\lambda$ = 1.5418 Å). The solid-state and solution UV-Vis spectra were recorded on a Bio-Logic MOS-500 multifunctional circular dichroism spectrometer. The solution UV-Vis absorption spectra were conducted by Agilent Cary 4000 UV-Vis spectrophotometer. $^{1}$H Nuclear Magnetic Resonance ($^{1}$H NMR) spectra were measured using a Bruker AVANCE III HD 400 (400 MHz) equipment. The GC-MS data were measured by the Agilent 5977B. Electron paramagnetic resonance (EPR) signals were recorded on a Bruker A300 spectrometer (Germany) at room temperature under visible-light irradiation using a 300 W Xe lamp. Scanning electron microscope (SEM) and energy-dispersive X-ray (EDX) analyses were monitored on the EM-30 AX PLUS (South Korea, COXEM company). Inductively coupled plasma-atomic emission spectroscopy (ICP-AES) was performed on Thermo Scientific iCAP 7000. X-ray photoelectron spectroscopy (XPS) was recorded on the Thermo Fisher K-Alpha+ instrument (UK). Steady-state photoluminescence spectra for the sample was recorded on a Horiba FluoroMax-4 fluorometer. Decay curve was recorded on an Edinburgh FLS920 spectrometer equipped with a NanoLED-455 flash lamp. The absolute photoluminescence quantum yield was measured on the Hamamatsu C11347-01 absolute PL quantum yield spectrometer. Photochemical reactions were performed with a LED flow reactor WP-TEC-1020HSL (WATTCAS, China).

**Syntheses of ligand**

The synthesis of organic ligand pytpy (4'-(pyridin-4-yl)-2,2':6',2"-terpyridine) and metalloligand Ru(pytpy)$_2$(PF$_6$)$_2$ has been slightly changed based on the literature.[S1]

**Intermediate A$_1$**

A mixture of 2-acetylpyridine (2.0 g, 15.6 mmol), pyridine (20.0 mL), iodine (4.6 g, 17.6 mmol) was refluxed under nitrogen at 100 °C for 3 h, then cooled to room temperature. The precipitate was filtered off, washed with ether and ethanol, and dried in vacuo. The product was a gray precipitate with good yield (4.3 g, 54%). $^1$H NMR (400 MHz, CDCl$_3$): $\delta$ 8.84 (d, $J$ = 3.7 Hz, 1H), 8.55 (d, $J$ = 16.0 Hz, 1H), 8.30 (t, $J$ = 7.5 Hz, 3H), 8.09-7.89 (m, 4H), 7.72-7.59 (m, 1H).
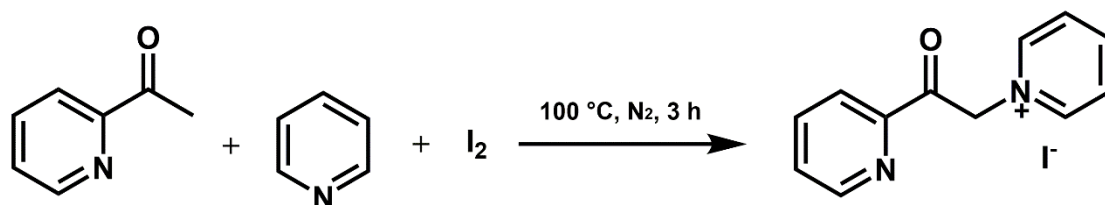


**Fig. S1** Synthesis of A$_1$.

**ligand A$_2$**

A mixture of sodium hydroxide solution (2.5 mL, 10%) with 4-pyridinecarboxaldehyde (4.3 g, 40.0 mmol) into 50 mL of ethanol. After the temperature was lowered to 0 °C, 2-acetylpyridine (4.9 g, 40 mmol) was added dropwise, then the reaction system was stirred for 3 h. The precipitate was collected, washed with ethanol, and dried to obtain a white powder (3.5 g, 41.7% yield). $^1$H NMR (400 MHz, CDCl$_3$): $\delta$ 8.67 (d, $J$ = 4.3 Hz, 1H), 8.51 (dd, $J$ = 4.7, 1.5 Hz, 1H), 7.99 (d, $J$ = 7.8 Hz, 1H), 7.84 (td, $J$ = 7.7, 1.7 Hz, 1H), 7.62-7.47 (m, 1H), 7.44 (d, $J$ = 6.2 Hz, 1H), 3.82 (dt, $J$ = 26.3, 13.2 Hz, 1H), 3.76-3.57 (m, 1H).
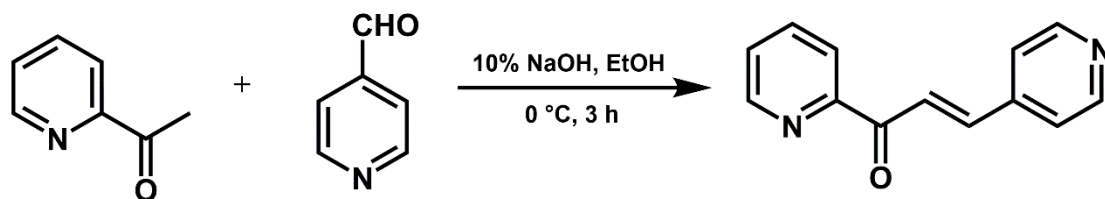
[S1] J. E. Beves, E. C. Constable, C. E. Housecroft, C. J. Kepert and D. J. Price, *CrystEngComm*, 2007, **9**, 456.

**Fig. S2** Synthesis of A$_2$.


**ligand pytpy**

A mixture of A$_1$ (2.2 g, 6.7 mmol), A$_2$ (1.4 g, 6.7 mmol) and ammonium acetate (3.1 g, 40.3 mmol) into 100 mL of methanol. Refluxing for 5 h, the precipitate was obtained after cooling to room temperature. The precipitate was filtered, washed with methanol and dried in vacuo to obtain a white sample (1.1 g, 52.9% yield). $^1$H NMR (400 MHz, CDCl$_3$): $\delta$ 8.86-8.80 (m, 4H), 8.77 (d, $J$ = 4.6 Hz, 2H), 8.72 (d, $J$ = 8.0 Hz, 2H), 7.96 (d, $J$ = 7.6 Hz, 2H), 7.92 (d, $J$ = 6.2 Hz, 2H), 7.43 (dd, $J$ = 7.2, 5.0 Hz, 2H).
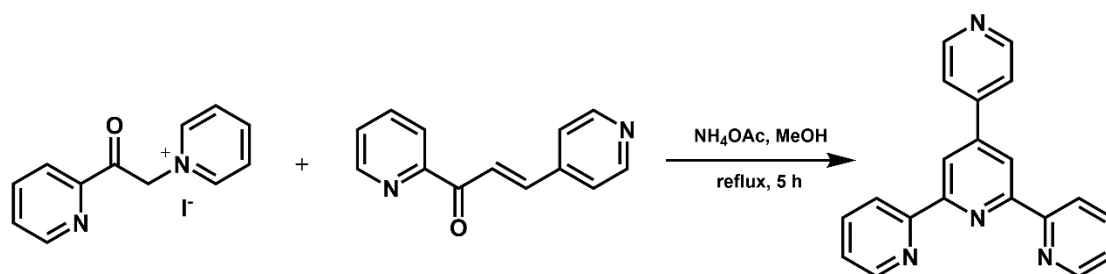


**Fig. S3** Synthesis of pytpy.


**Metalloligand Ru(pytpy)$_2$(PF$_6$)$_2$**

RuCl$_2$(DMSO)$_4$ (0.97 g, 2 mmol) and pytpy (1.24 g, 4 mmol) were mixed and dissolved in ethylene glycol to reflux for 3 hours. After cooling to room temperature, deionized water and ammonium hexafluorophosphonate were added to produce dark red precipitate. After filtration, the product was washed with water and dichloromethane, dried in vacuo to give the powdery sample (1.25 g, 62% yield). FT-IR spectrum (KBr, pellets, cm$^{-1}$): 3373(m), 3055(w), 1596(s), 1409(s), 820(s). $^1$H NMR (400 MHz, CD$_3$CN): $\delta$ 9.09 (s, 1H), 9.00 (d, $J$ = 5.6 Hz, 1H), 8.69 (d, $J$ = 8.1 Hz, 1H), 8.16 (d, $J$ = 5.7 Hz, 1H), 8.00 (t, $J$ = 7.8 Hz, 1H), 7.45 (d, $J$ = 5.4 Hz, 1H), 7.29-7.18 (m, 1H).
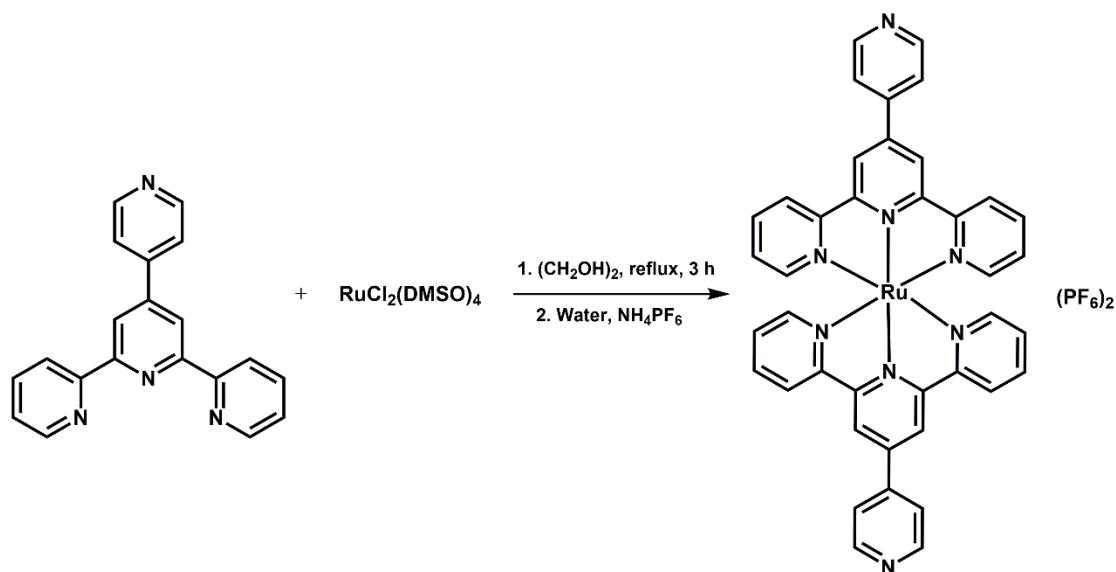
**Fig. S4** Synthesis of Ru(pytpy)$_2$(PF$_6$)$_2$.

## Syntheses of RuZn-MMOF-1

A mixture of Zn(NO$_3$)$_2$·6H$_2$O (11.9 mg, 0.04 mmol), Ru(pytpy)$_2$(PF$_6$)$_2$ (20.2 mg, 0.02 mmol), 2,6-naphthalene dicarboxylic acid (8.6 mg, 0.04 mmol) and DMF/EtOH mixed solvent (4 mL, 2:1, v/v) was added in 10 mL sealed Pyrex glass tube. It was placed in an oven with a temperature of 120 ℃ for 72 h, then the reaction system was reduced to room temperature at a rate of 5 °C h$^{-1}$. The product was filtered and washed with DMF, MeOH, respectively. The red block crystals were obtained, then the sample was soaked in ethanol, exchanged at room temperature for three days, and dried under vacuum at 50 °C for 12 h (20.3 mg, 62.4% yield based on the Ru(pytpy)$_2$(PF$_6$)$_2$). FT-IR spectrum (KBr, pellets, cm$^{-1}$): 3409(m), 3055(w), 2012(w), 1609(s), 1383(s), 1006(m), 784(s), 611(w). Element analysis (CHN): C$_{70}$H$_{58}$F$_6$N$_9$O$_{14}$PRuZn$_2$ (corresponding to {[RuZn$_2$(pytpy)(NDC)$_2$]NO$_3$·PF$_6$·3C$_2$H$_5$OH}$_n$), calculated (%): C 51.71, H 3.60, N 7.75; found (%): C 51.68, H 3.66, N 7.36.

## Crystal Structure Analysis

### Crystallographic Studies

Single crystal structures of RuZn-MMOF-1 was measured by X-ray diffraction at 100 K. Data collections were performed on an Oxford Diffraction XtalAB [Rigaku (Cu) X-ray dual wavelength source, K$\alpha$, $\lambda$ = 1.5418 Å] equipped with a monochromator and CCD plate detector (CrysAlisPro CCD, Oxford Diffraction Ltd). The crystallographic calculations were performed using the SHELXL-2018/3.[S2] The structure was solved by direct methods and refined by full-matrix least-squares refinements based on $F^2$. Anisotropic thermal parameters were applied to all non-hydrogen atoms. The hydrogen atoms were generated geometrically. The crystal structure contains lots of unknow residual electron density belong to guest molecules and/or counter anions. The treatment for the guest molecules and partial free counter anions in the pore channel involves the use of the SQUEEZE program of PLATON,[S3] which can provide a better refinement data. A summary of crystal data and structure refinement parameters is listed in Table S1. CCDC no. 2026257.

[S2] (a) G. M. Sheldrick, *Acta Crystallogr., Sect. A: Found. Crystallogr.*, 2008, **64**, 112; (b) C. B. Hubschle, G. M. Sheldrick and B. Dittrich, *J. Appl. Cryst.*, 2011, **44**, 1281; (c) G. M. Sheldrick, *Acta Cryst.*, 2015, **C71**, 3.

[S3] A. L. Spek, *Acta Cryst.*, 2015, **C71**, 9.

**Table S1** Crystal Data and Structure Refinement Parameters for RuZn-MMOF-1.

| Parameter | RuZn-MMOF-1 |
|---|---|
| Chemical formula | $C_{64}H_{40}N_8O_8RuZn_2$ |
| Formula weight | 1280.85 |
| Crystal system | Tetragonal |
| Space group | $P4_2/nnm$ |
| $a$ (Å) | 13.0880 (1) |
| $b$ (Å) | 13.0880(1) |
| $c$ (Å) | 24.9634(4) |
| $\alpha$ (deg) | 90 |
| $\beta$ (deg) | 90 |
| $\gamma$ (deg) | 90 |
| $V$ (Å$^3$) | 4276.12(9) |
| $Z$ | 2 |
| $D_{calcd}$(g cm$^{-3}$) | 0.995 |
| $\mu$ (mm$^{-1}$) | 2.417 |
| Reflections collected | 14475 |
| Unique reflections | 2374 |
| $R_{int}$ | 0.0319 |
| Goodness-of-fit on $F^2$ | 1.133 |
| $R_1$[a] [I > 2σ(I)] | 0.0562 |
| $wR_2$[b] [I > 2σ(I)] | 0.1870 |
| $R_1$[a] [all refl.] | 0.0586 |
| $wR_2$[b] [all refl.] | 0.1888 |
| CCDC number | 2026257 |

[a] $R_1 = \sum(||F_0| - |F_c||)/\sum|F_0|$; [b] $wR_2 = [\sum w(F_0{}^2 - F_c{}^2)^2/\sum w(F_0{}^2)^2]^{1/2}$

# Structural Analysis and Additional Characterization
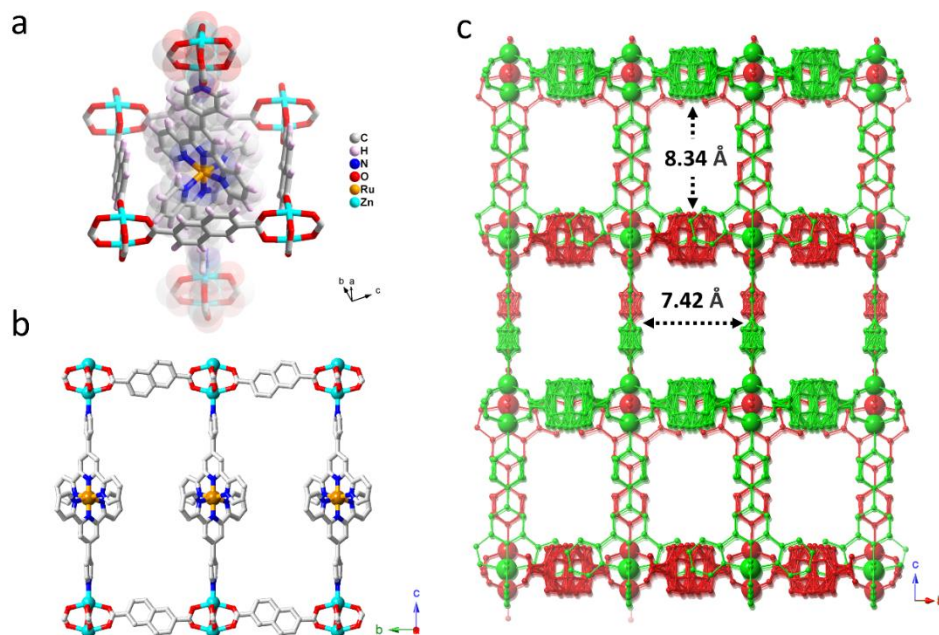


**Fig. S5** (a) The coordination environment of the Ru and Zn metal centers of RuZn-MMOF-1. (b) Partial view of the single-fold structure of the RuZn-MMOF-1 (direction of the *a* axis). (c) Pore channel window of the RuZn-MMOF-1 with the size of about $7.42 \times 8.34$ Å$^2$ (the structure has serious symmetry disorder, and no atom is hidden in the figure). H atoms are omitted for clarity.
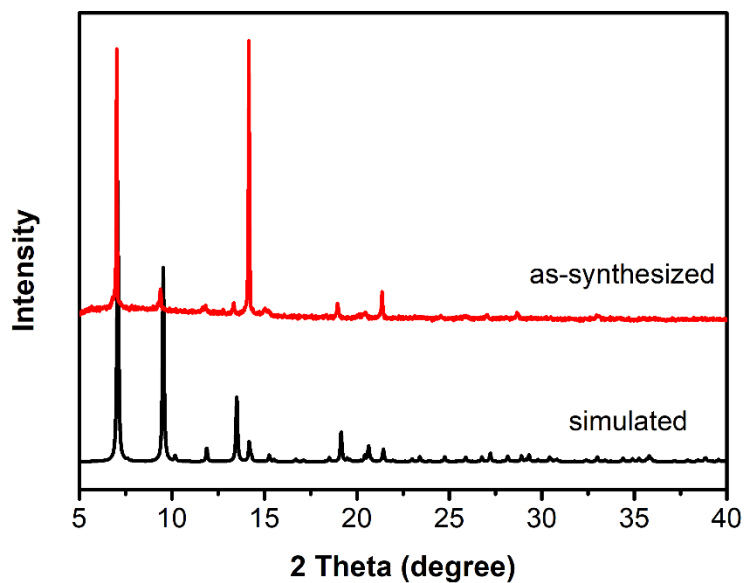
**Fig. S6** PXRD patterns of simulated and as-synthesized RuZn-MMOF-1.
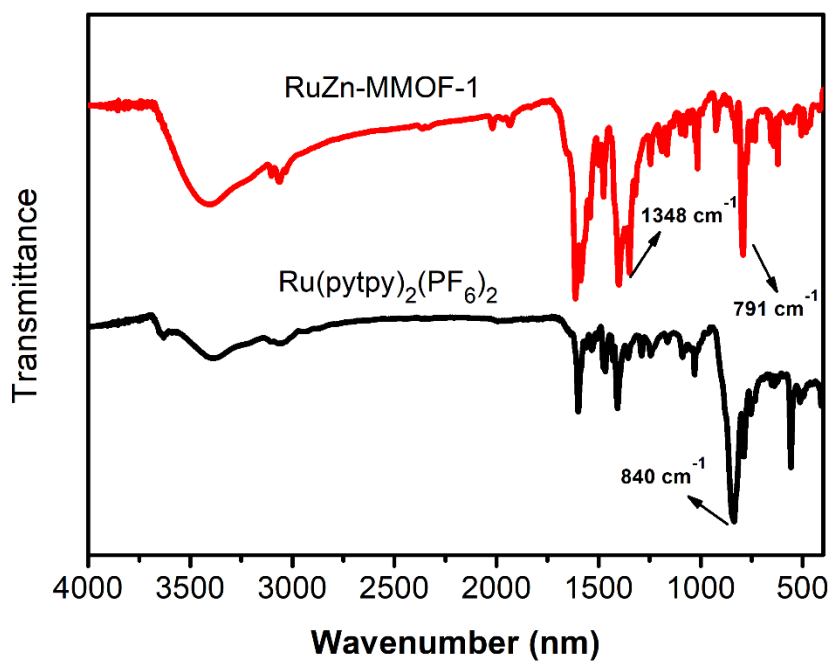


**Fig. S7** FT-IR spectra of RuZn-MMOF-1 and Ru(pytpy)$_2$(PF$_6$)$_2$. The characteristic peaks of NO$_3^-$ (about 1384 cm$^{-1}$) and PF$_6^-$ (about 791 cm$^{-1}$ or 840 cm$^{-1}$) in different samples are marked.
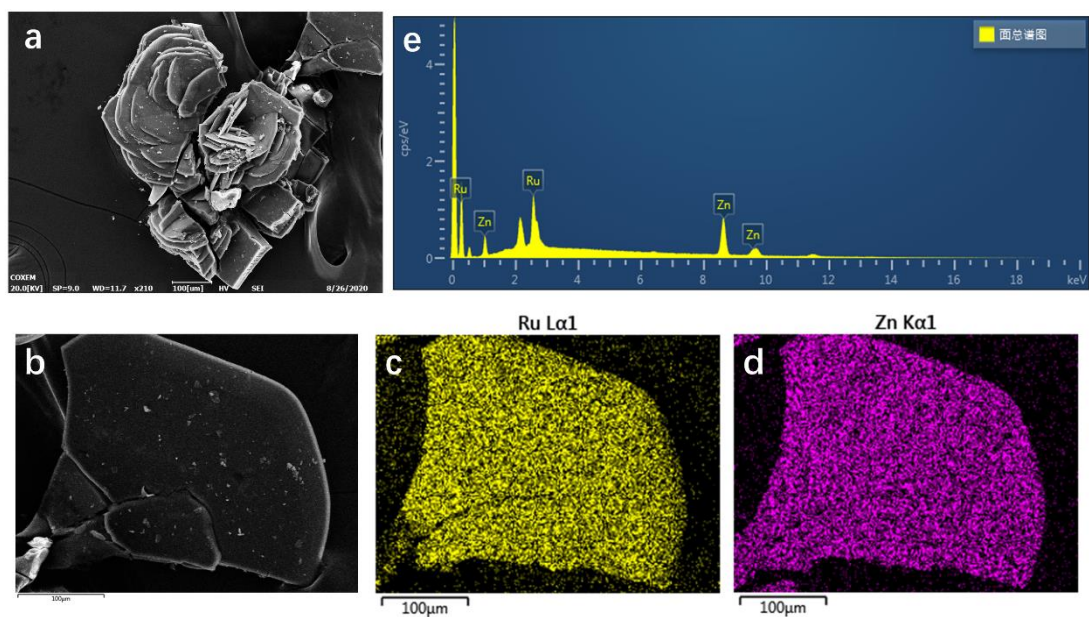
**Fig. S8** (a,b) SEM, (c,d) EDX elemental mapping and (e) EDX elemental analysis of activated RuZn-MMOF-1.

**Table S2**. ICP-AES results for RuZn-MMOF-1.

| entry | Zn (ppm) | Ru (ppm) | Zn/Ru (molar ratio) |
|-------|----------|----------|---------------------|
| 1 | 0.805 | 0.586 | 2.131 |
| 2 | 0.799 | 0.592 | 2.096 |
| 3 | 0.769 | 0.552 | 2.162 |
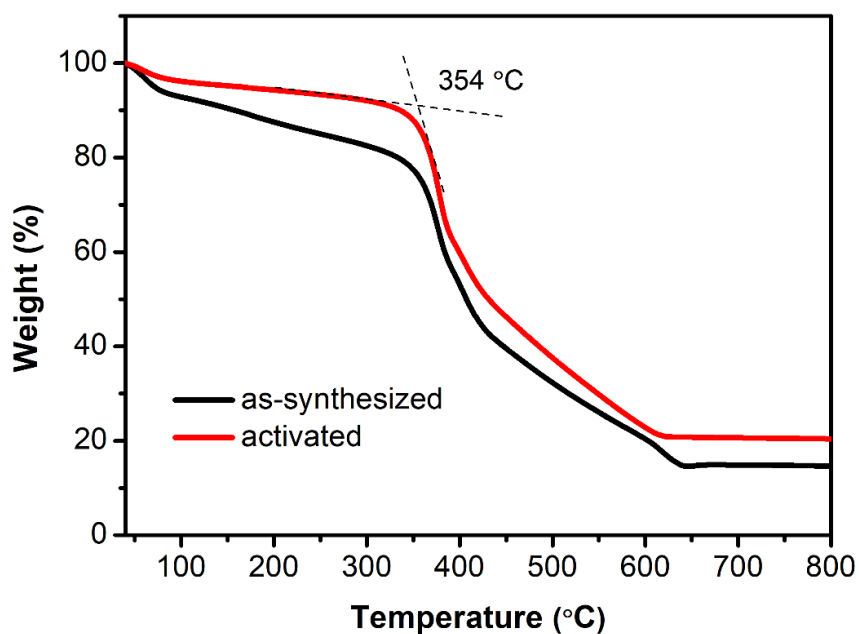
**Fig. S9** TGA of as-synthesized and activated RuZn-MMOF-1 under $N_2$ atmosphere.
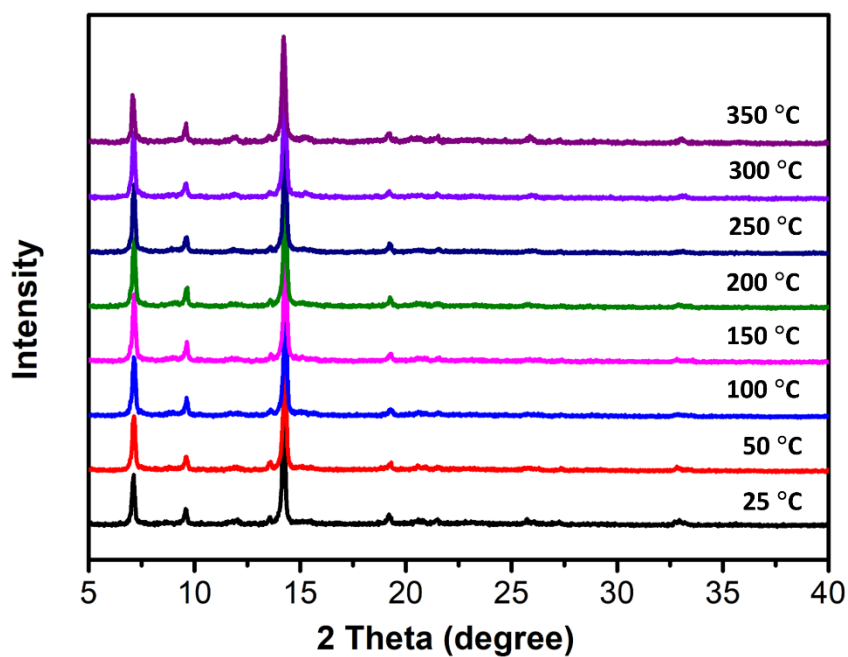


**Fig. S10** Variable temperature PXRD pattern (VT-PXRD) of RuZn-MMOF-1 under air atmosphere.
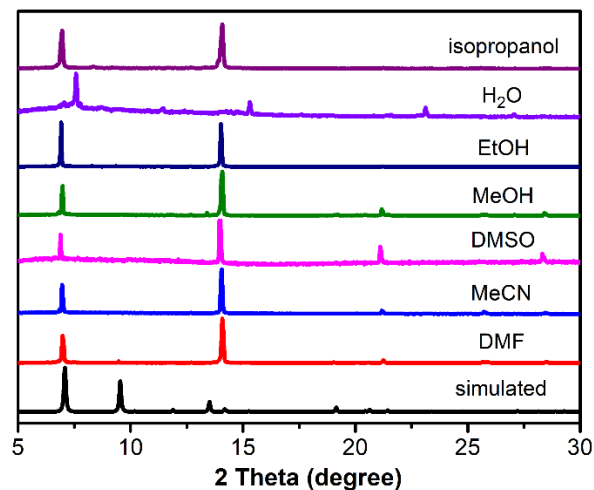
**Fig. S11** PXRD patterns of RuZn-MMOF-1 expose in air or soak in virous solvents for 5 days at room temperature.
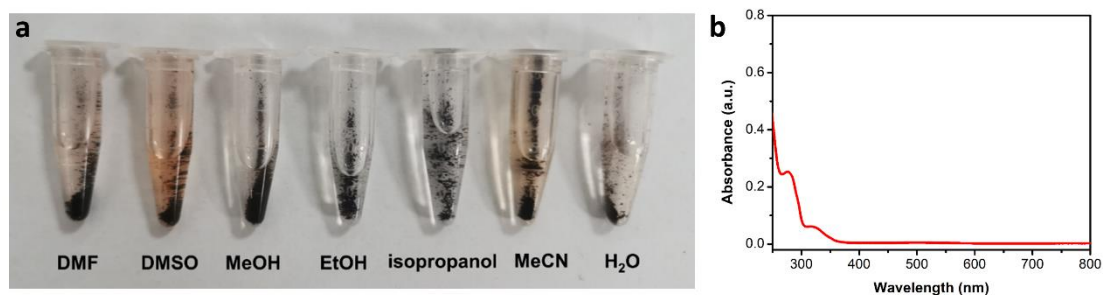


**Fig. S12** (a) Photographs of RuZn-MMOF-1 soaked in virous solvents for 5 days at room temperature. (b) UV-Vis spectrum of the supernatant of RuZn-MMOF-1 soaked in isopropanol for 5 days at room temperature.
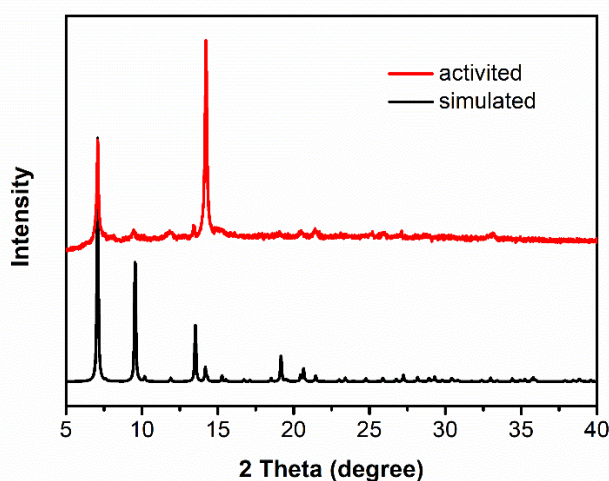


**Fig. S13** PXRD pattern of activated RuZn-MMOF-1. Activated condition: the sample is soaked in isopropanol, exchanged at room temperature for three days (change fresh solvent once a day), and dried under vacuum at 100 °C for 12 h.
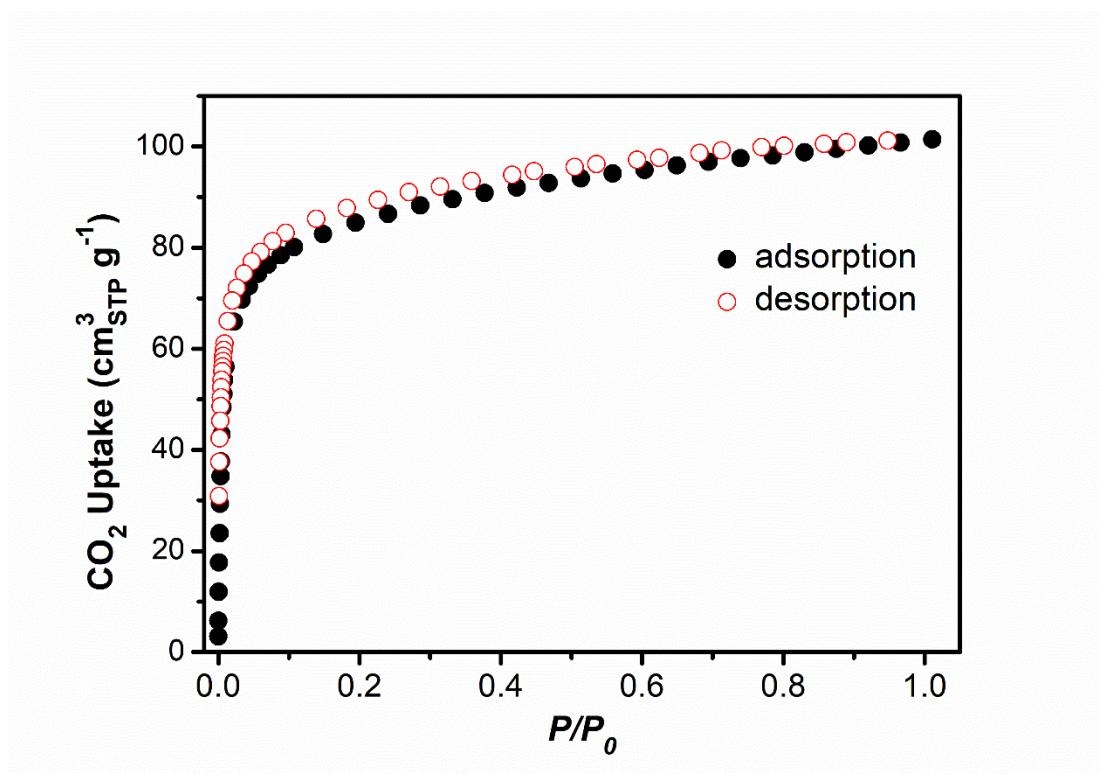
**Fig. S14** $CO_2$ adsorption/desorption isotherm of RuZn-MMOF-1 at 196 K.
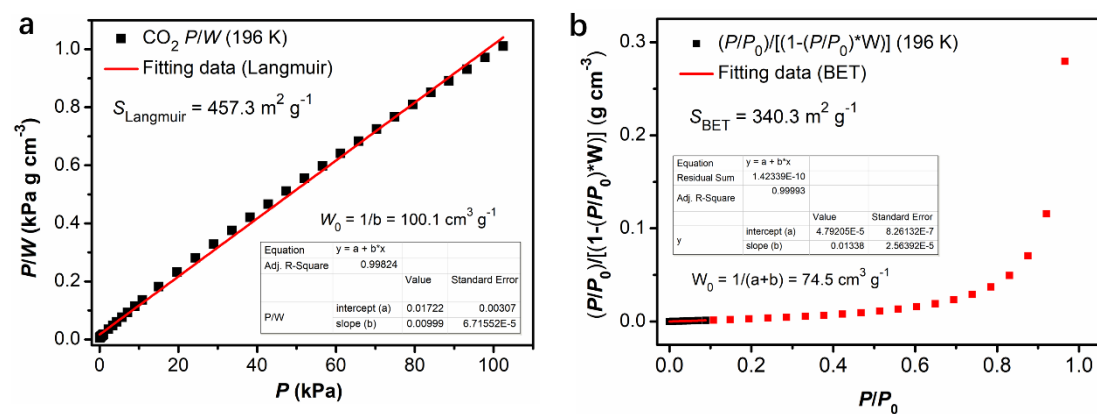


**Fig. S15** (a) Langmuir and (b) BET surface area are calculated by using the data of $CO_2$ adsorption isotherm at 196 K based on the reported literature.[S4]

S4  W. Yang, A. J. Davies, X. Lin, M. Suyetin, R. Matsuda, A. J. Blake, C. Wilson, W. Lewis, J. E. Parker, C. C. Tang, M. W. George, P. Hubberstey, S. Kitagawa, H. Sakamoto, E. Bichoutskaia, N. R. Champness, S. Yang and M. Schroder, *Chem. Sci.*, 2012, **3**, 2993.

**Table S3.** Fitting data of the photoluminescence decay of (1) RuZn-MMOF-1 and (2) Ru(pytpy)$_2$(PF$_6$)$_2$

| | A1 | A2 | A3 | $\tau_1$ | $\tau_2$ | $\tau_3$ | $\tau_{av}$ | Chi2 |
|---|---|---|---|---|---|---|---|---|
| (1) | $2.59 \times 10^{-4}$ | $3.57 \times 10^{-4}$ | 3.17 | 5.11 | 94.04 | 0.03 | 22.09 | 1.62 |
| (2) | $6.71 \times 10^{-5}$ | 0.68 | / | 17.21 | 0.01 | / | 0.39 | 1.34 |

$\tau_{av} = (A1 \times \tau_1{}^2 + A2 \times \tau_2{}^2 + A3 \times \tau_3{}^2)/(A1 \times \tau_1 + A2 \times \tau_2 + A3 \times \tau_3)$.

## Photocatalytic experiments

### EPR measurement

The 10 mg of RuZn-MMOF-1 powder was dispersed in 5 ml of isopropanol, and then the mixture was sonicated for homogeneous dispersion. Next, the 200 $\mu$L of suspended sample and 100 $\mu$L of TEMPO solution (concentration of 100 mM) were mixed, and then the mixture was put into a capillary tube for measurement, using 300 W xenon lamp for light source.

### Photooxidation of 1,3-diphenylisobenzofuran (1,3-DPBF) and 1,5-dihydroxynaphthalene (1,5-DHN)

Taking 3 mL isopropanol solution of a specific concentration of 1,3-DPBF ($3 \times 10^{-5}$ mol/L) or 1,5-DHN ($1 \times 10^{-4}$ mol/L) in a quartz tube, then adding 20 mg of RuZn-MMOF-1 into the reaction system. The reaction was placed in the photochemical reaction system with 10 W white LED as light source. During the reaction process, the reaction solution was moved out for the UV-visible absorption monitoring at the specific time.

### Photooxidation of CEES to CEESO and CEESO$_2$

Adding 0.2 mmol 2-chloroethyl ethyl sulfide (CEES), 0.01 mmol RuZn-MMOF-1 as catalyst (about 15 mg), 0.02 mmol internal reference (naphthalene), and 2 mL isopropanol ($^i$ProOH) into a quartz tube, then the mixture was placed in the photochemical reaction system with 10 W white LED as light source. During the reaction process, the part of reaction solution was moved out and diluted for detecting the conversion of substrates by gas chromatography-mass spectrometry (GC-MS). The reaction by using Ru(pytpy)$_2$(PF$_6$)$_2$ (0.01 mmol) as the catalyst, as well as the control reaction and the blank experiment were all carried out under the same experimental conditions.
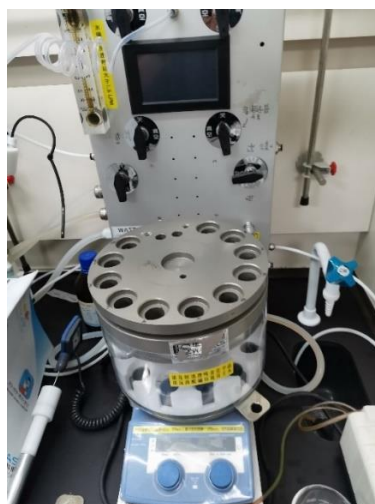
**Fig. S16** The WP-TEC-1020HSL photochemical reaction system with the white light LED (10 W) flow reactor is used to perform the photooxidation of the sulfur mustard simulant under room temperature.
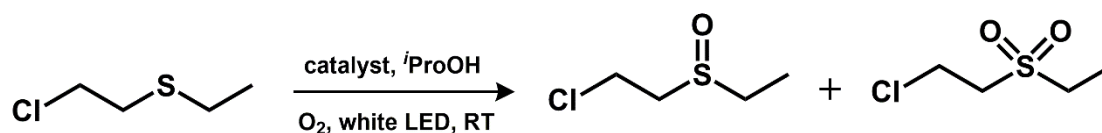


**Fig. S17** Chemical reaction illustration of photocatalytic oxidation of CEES to CEESO and CEESO$_2$.
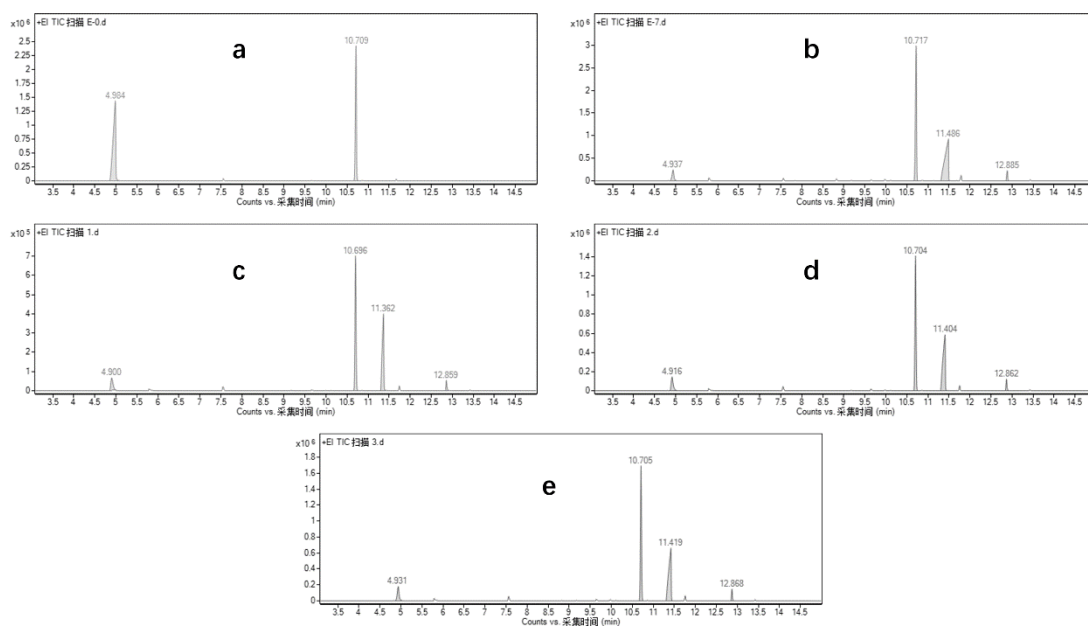


**Fig. S18** Gas chromatograms of the reaction systems (a) before and (b-e) after the photocatalytic cycles.
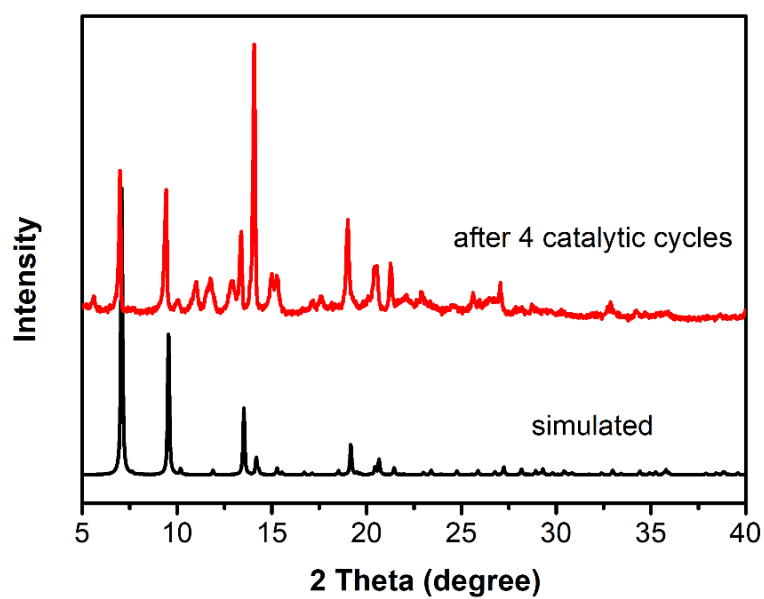
**Fig. S19** The PXRD patterns of RuZn-MMOF-1 after 4 photocatalytic cycles.
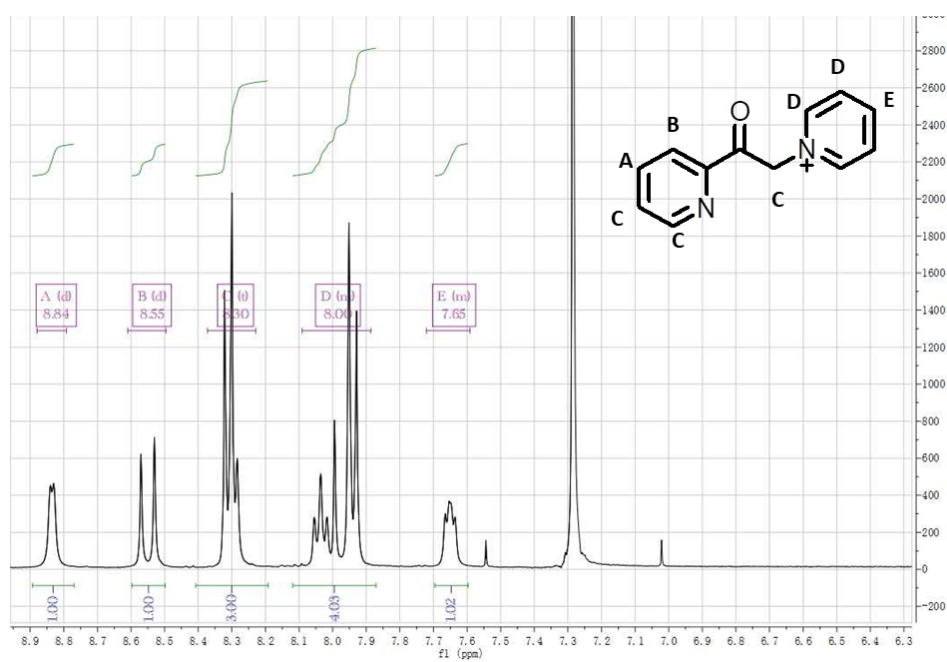


**Fig. S20** $^1$H NMR (400 MHz) spectrum for A$_1$ (CDCl$_3$, 298 K).
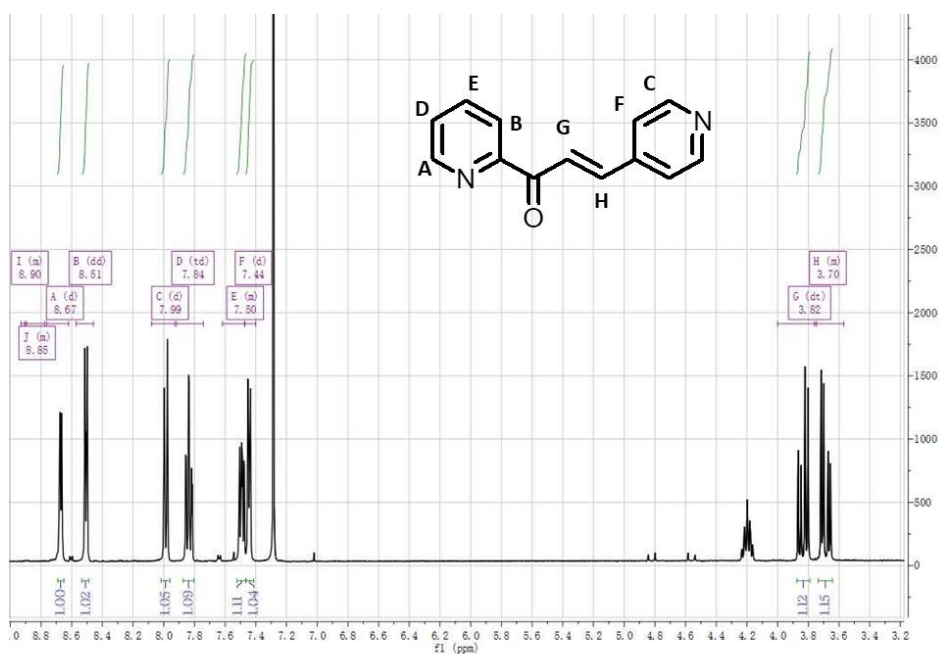
**Fig. S21** ¹H NMR (400 MHz) spectrum for A₂ (CDCl₃, 298 K).
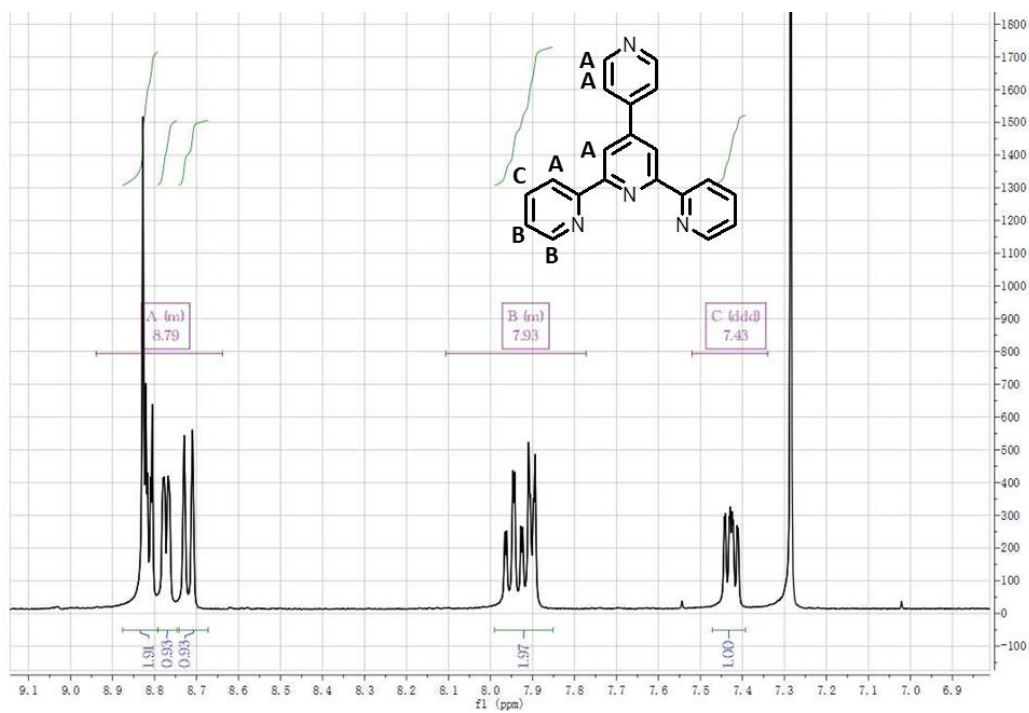


**Fig. S22** ¹H NMR (400 MHz) spectrum for pytpy (CDCl₃, 298 K).
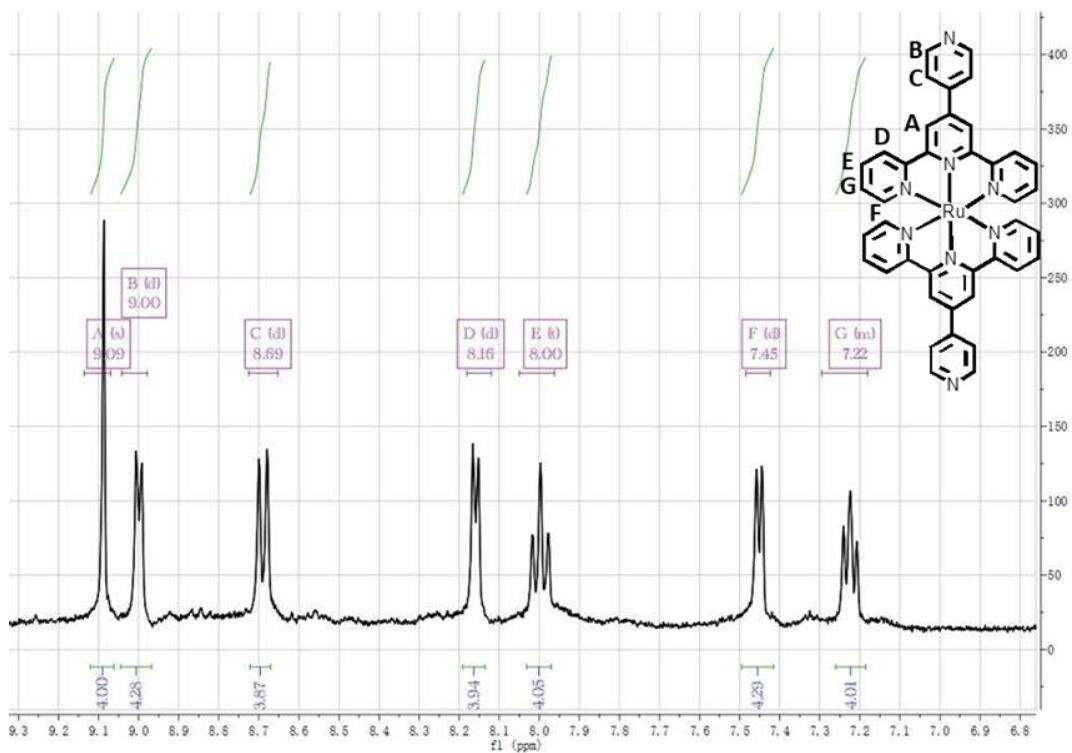
**Fig. S23** ¹H NMR (400 MHz) spectrum for Ru(pytpy)₂(PF₆)₂ (CD₃CN, 298 K).

## Computational Details

### Reduced density gradient (RDG) analysis

The intricate noncovalent interactions between the Ru(pytpy)$_2$$^{2+}$ motif and NDC$^{2-}$-based square grid were visualized through reduced density gradient (RDG) analysis based on electron density distribution.[S5] On the RDG isosurfaces, green color refers to van der Waals interaction; blue color suggests the strongest attractions, such as hydrogen and halogen bonds. The steric hindrance goes stronger from brown to red. The RDG isosurfaces were calculated by *Multiwfn* program[S6] and drawn by VMD 1.9.3.[S7] The RDG isosurface was limited to the cubic space surrounding Ru(II) of Ru(pytpy)$_2$$^{2+}$ motif with extending distance of 12.0 Bohr in X, Y, Z direction, respectively, and the total grid numbers are high quality one with 1728000.

### DFT/TDDFT calculation

Density functional theory (DFT) and time-dependent DFT (TDDFT) calculations were performed to shed some light on the mechanism of this photocatalytic reaction. The $\omega$B97XD functional[S8] was adopted with the effective core potential (ECP) of LanL2dz basis set[S9] for metals and 6-311G** basis set[S10] for non-metals. All calculations were carried out using Gaussian 09 software package[S11] and some of the output files were used as input files of Multiwfn 3.6 software packages[S12] to draw the contours of molecular orbitals (isovalue = 0.02) and electron density difference (EDD)

[S5] E. R. Johnson, S. Keinan, P. Mori-Sánchez, J. Contreras-García, A. J. Cohen and W. Yang, *J. Am. Chem. Soc.*, 2010, **132**, 6498.

[S6] T. Lu and F. Chen, *J. Comput. Chem.*, 2012, **33**, 580.

[S7] W. Humphrey, A. Dalke and K. Schulten, *J. Mol. Graphics*, 1996, **14**, 33.

[S8] J. D. Chai and M. Head-Gordon, *Phys. Chem. Chem. Phys.*, 2008, **10**, 6615.

[S9] (a) T. H. Dunning Jr. and P. J. Hay, *In Modern Theoretical Chemistry*; Schaefer, H. F., III., Ed., Plenum: New York, 1976; (b) P. J. Hay and W. R. J. Wadt, *Chem. Phys.*, 1985, **82**, 270; (c) W. R. Hadt and P. J. J. Hay, *Chem. Phys.*, 1985, **82**, 284; (d) P. J. Hay and W. R. J. Wadt, *Chem. Phys.*, 1985, **82**, 299.

[S10] (a) R. Krishnan, J. S. Binkley, R. Seeger and J. A. Pople, *J. Chem. Phys.*, 1980, **72**, 650; (b) A. D. McLean and G. S. Chandler, *J. Chem. Phys.*, 1980, **72**, 5639.

[S11] M. J. Frisch, G. W. Trucks, H. B. Schlegel, G. E. Scuseria, M. A. Robb, J. R. Cheeseman, G. Scalmani, V. Barone, B. Mennucci, G. A. Petersson, H. Nakatsuji, M. Caricato, X. Li, H. P. Hratchian, A. F. Izmaylov, J. Bloino, G. Zheng, J. L. Sonnenberg, M. Hada, M. Ehara, K. Toyota, R. Fukuda, J. Hasegawa, M. Ishida, T. Nakajima, Y. Honda, O. Kitao, H. Nakai, T. Vreven, Jr. J. A. Montgomery, J. E. Peralta, F. Ogliaro, M. Bearpark, J. J. Heyd, E. Brothers, K. N. Kudin, V. N. Staroverov, R. Kobayashi, J. Normand, K. Raghavachari, A. Rendell, J. C. Burant, S. S. Iyengar, J. Tomasi, M. Cossi, N. Rega, J. M. Millam, M. Klene, J. E. Knox, J.B. Cross, V. Bakken, C. Adamo, J. Jaramillo, R. Gomperts, R. E. Stratmann, O. Yazyev, A. J. Austin, R. Cammi, C. Pomelli, J. Ochterski, R. L. Martin, K. Morokuma, V. G. Zakrzewski, G. A. Voth, P. Salvador, J. J. Dannenberg, S. Dapprich, A. D. Daniels, O. Farkas, J. B. Foresman, J. V. Ortiz, J. Cioslowski and D. J. Fox, Gaussian 09 (Revision E.01), Gaussian, Inc., Wallingford, CT, 2013.

[S12] T. Lu and F. W. Chen, *J. Comp. Chem.*, 2012, **33**, 580.

maps (isovalue = $4.0 \times 10^{-4}$ a.u.).

The simplified model for computations were taken from the X-ray crystal structure of RuZn-MMOF-1 at 100 K and denoted as $Ru(pytpy)_2$-ZnPh. This model has taken into account the whole coordination environments around Ru and Zn, and the $PhCOO^-$ in the paddle-wheel $Zn_2(PhCOO)_4$ coordination units was simplified from 2,6-naphthalene dicarboxylic acid.
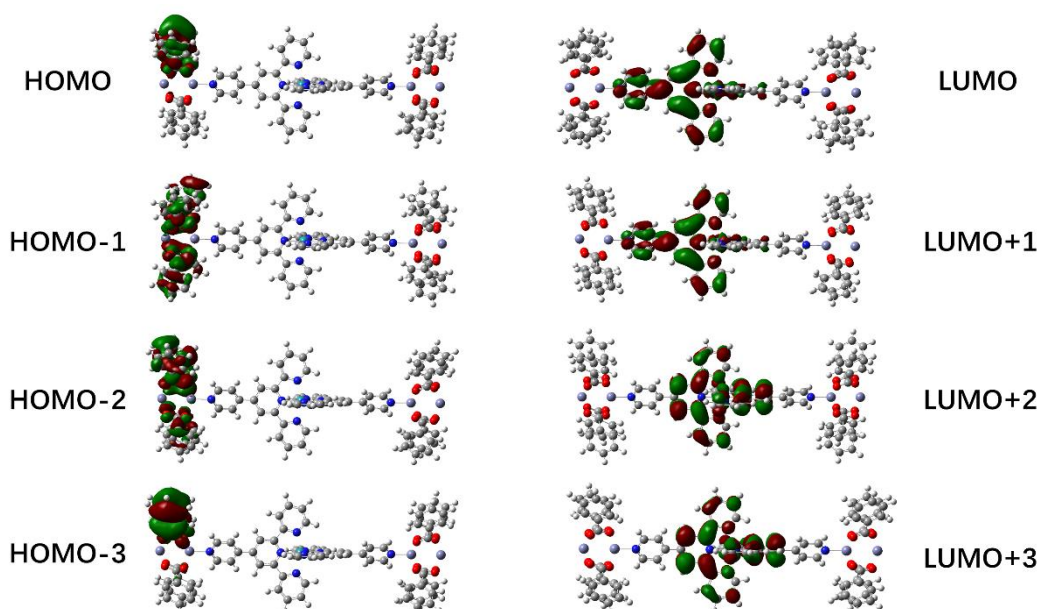


**Fig. S24** The frontier molecular orbitals (isovalue = 0.02). The HOMO to HOMO-3 have π-bonding orbitals of the model $PhCOO^-$ motifs. The LUMO to LUMO+3 are mainly π* orbitals delocalized on the pytpy ligands and Ru orbital characteristics.

**Table S4** TDDFT results of selected $S_0 \rightarrow S_n$ transitions for Ru(pytpy)$_2$-ZnPh model

| No. | $\lambda$ (nm) | E (eV) | $f$ | EDD | Assignment |
|-----|------|--------|-----|-----|------------|
| 1 | 505.1 | 2.456 | 0.0072 | | [1]LLCT |
| 2 | 489.6 | 2.534 | 0.0017 | | [1]LLCT |
| 3 | 460.1 | 2.697 | 0.0003 | | [1]LLCT |
| 4 | 441.2 | 2.812 | 0.0001 | | [1]LLCT |
| 5 | 434.3 | 2.857 | 0.0019 | | [1]LLCT |
| 6 | 430.1 | 2.885 | 0.0002 | | [1]LLCT |
| 7 | 426.5 | 2.909 | 0.0001 | | [1]LLCT |
| 8 | 426.0 | 2.912 | 0.0000 | | [1]LLCT |
| 9 | 422.8 | 2.934 | 0.0002 | | [1]LLCT |
| 10 | 421.9 | 2.940 | 0.0010 | | [1]LLCT |
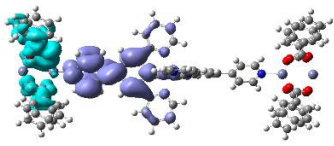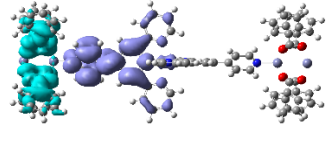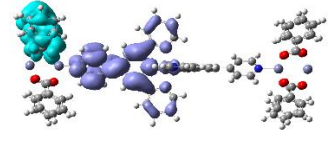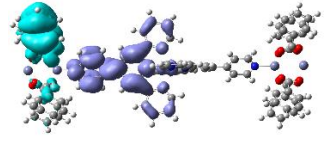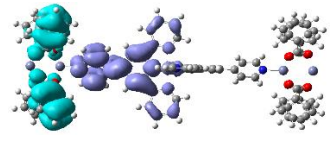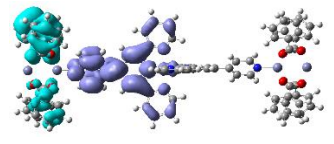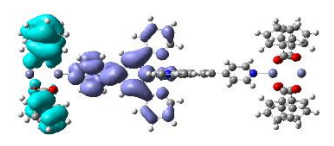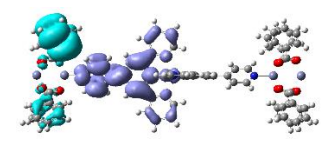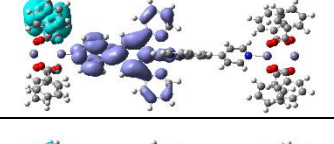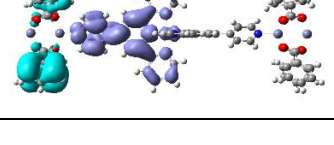
**Table S5** TDDFT results of selected $S_0 \rightarrow T_n$ transitions for Ru(pytpy)$_2$-ZnPh model
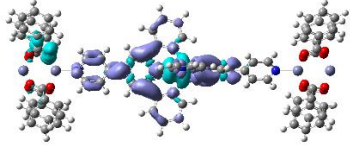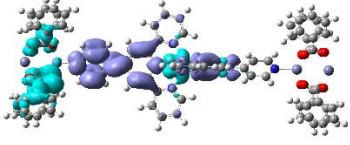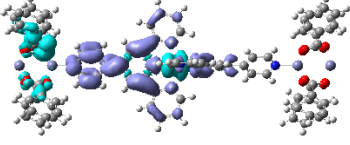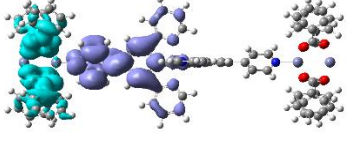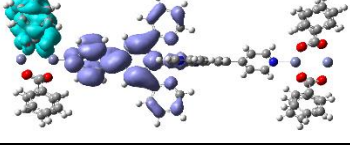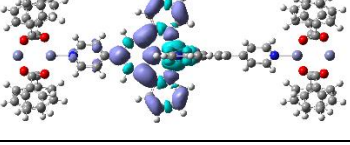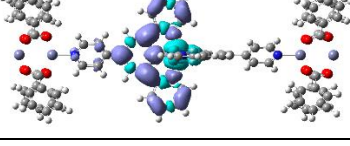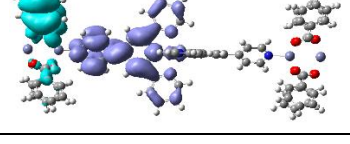
| No. | λ (nm) | E (eV) | EDD | Assignment |
|---|---|---|---|---|
| 1 | 513.6 | 2.416 | | $^3$MLCT $^3$LLCT |
| 2 | 507.3 | 2.446 | | $^3$MLCT $^3$LLCT |
| 3 | 502.0 | 2.472 | | $^3$MLCT $^3$LLCT |
| 4 | 489.9 | 2.532 | | $^3$LLCT |
| 5 | 460.3 | 2.696 | | $^3$LLCT |
| 6 | 444.2 | 2.793 | | $^3$MLCT $^3$ILCT |
| 7 | 443.6 | 2.797 | | $^3$MLCT $^3$ILCT |
| 8 | 441.4 | 2.811 | | $^3$LLCT |
| 9 | 434.5 | 2.856 | | $^3$LLCT |
| 10 | 430.1 | 2.884 | | $^3$LLCT |